lubricants

MDPI

Article

Comparative Studies on the Dry Sliding Behavior of a Low-Metallic Friction Material with the Addition of Graphite and Exfoliated g-C_3N_4

Priyadarshini Jayashree [1], Vlastimil Matějka [2], Kryštof Foniok [2] and Giovanni Straffelini [1,*]

[1] Department of Industrial Engineering, University of Trento, Via Sommarive 9, 38123 Trento, Italy; priyadarshini.jayashree@unitn.it
[2] Department of Chemistry, Faculty of Materials Science and Technology, VŠB—Technical University of Ostrava, 17. Listopadu 2172/15, 70833 Ostrava, Czech Republic; vlastimil.matejka@vsb.cz (V.M.); krystof.foniok@vsb.cz (K.F.)
* Correspondence: giovanni.straffelini@unitn.it

Abstract: This study compares the effect of the addition of two types of lubricants on the dry sliding behavior of a simplified Cu-free phenolic resin-based composite material. The lubricants were commercial graphite and exfoliated graphitic carbon nitride (codenamed: TEX6). The graphite particles were rounded and of 'flaky' character. The TEX6 particles were not only flaky, but also irregular in shape, and 'fluffy'. Both lubricants were added individually in the basic formulation and subjected to dry sliding tests on pin-on-disc testing equipment in mild conditions and against a grey cast-iron counterface. The tests with TEX6 observed a stable steady state in the friction coefficient (CoF) with lower scatter and lower average friction coefficient and pin wear magnitude when compared to samples containing graphite. Additionally, the worn surfaces of the TEX6-containing samples had extremely smooth, compact, and continuous secondary plateau coverage when compared to the graphite-containing samples. The counterface paired with the TEX6-containing samples observed much lower abrasive action compared to the graphite-containing samples. Through the wear testing and further evaluation of the secondary plateaus, the possible addition of TEX6 as a lubricant in friction material composition was explained, making it a promising component for automotive braking applications.

Keywords: graphitic carbon nitride; graphite; lubricant; wear; friction; low-metallic friction materials

Citation: Jayashree, P.; Matějka, V.; Foniok, K.; Straffelini, G. Comparative Studies on the Dry Sliding Behavior of a Low-Metallic Friction Material with the Addition of Graphite and Exfoliated g-C_3N_4. *Lubricants* **2022**, *10*, 27. https://doi.org/10.3390/lubricants10020027

Academic Editor: Adolfo Senatore

Received: 11 January 2022
Accepted: 9 February 2022
Published: 15 February 2022

1. Introduction

The current commercially available friction materials for automotive braking applications can be roughly divided into low-metallic (LM), semi-metallic (SM), and non-asbestos organic (NAO) materials. These complex friction materials essentially constitute four types of ingredients: binders, friction modifiers, fillers, and reinforcements [1–8].

Low-metallic friction materials are known to be reinforced with significantly low metallic content (less than 30%), such as steel fibers or powders, brass powders, and copper fibers or powders [9–11]. Of course, the utilization of Cu has been restricted due to its adverse effects on the environment [2,12]. Reinforcements such as steel fibers are known to impart strength, wear resistance, and thermal diffusivity [13]. Additionally, steel fibers are known to act as primary plateaus, assisting in the formation of uniform and compact secondary plateaus, and improving the tribological behavior of the friction material [2,14,15]. Fillers such as barite ($BaSO_4$) and calcite ($CaCO_3$) have been found to reduce the wear rate and particulate emissions, and play a pivotal role in the formation of a stable friction layer in a wear system [12]. Furthermore, Aranganathan et al. [16] have demonstrated that the addition of aramid fibers in the friction materials promotes resistance to wear and friction stabilization [14].

The friction modifiers can be divided into abrasives and lubricants. Abrasives are added to the mix to provide frictional stability and to remove the pyrolyzed film formed on the surface of the counterface. Some of the widely used abrasives are zirconia, alumina, silicon carbide, silica, quartz, and zirconium silicate [17]. Boz et al. [13] have stated that the addition of alumina helped stabilize the friction traces. Tomášek et al. [18] demonstrated that the alumina addition elevated the friction coefficient magnitude and removed the negative wear rate in non-metallic friction materials.

The second type of friction modifier are lubricants, which protect the mating interfaces from excessive wear and reduce friction [17]. Amongst the variously known lubricants, metal sulfides and graphite are extensively employed in automotive friction materials. Metal sulfides (such as SnS_2, Cu_2S, Sb_2S_3, WS_2, MoS_2, Bi_2S_3) are especially known for their ability to control friction and wear. This is due to their lamellar structure, which assists in the formation of a robust friction/transfer layer on the mating surfaces with strong adhesion [19–22]. The metal sulfides can either be used individually or can be added in a mix in the composition [23]. Graphite is primarily known for its good lubrication characteristics, high thermal conductivity, reduction in excessive wear of contact surfaces by contributing towards the formation of the friction/tribo-layer, high damping, and superior seizure resistance [6,24]. Ertan et al. [25] have stated that the presence of graphite contributes to the frictional stability of a system and sustains the required friction coefficient magnitude at high-temperature testing conditions [17,26,27]. Cho et al. [17] have stated that the addition of graphite helps in improving fade resistance. Österle et al. [24] in their extensive review on different lubricants stated that the friction regime in composites with high graphite content was brought down from 'high' to 'low'. Zhang et al. [28] demonstrated that with the addition of graphite, a lubricating layer is deposited in the pits/grooves on the worn mating surfaces, which assists in the collection and compaction of wear debris. This leads to a decrease in the contact area between the surfaces, effectively resulting in stable friction and lower wear characteristics at different sliding speeds, temperature, and loading conditions. Cheng et al. [29] have stated that the lamellar structure and weak bonding between the atomic layers in graphite assists the shear between the adjacent layers, which helps the effective lubrication and reduction in the wear system.

Graphitic carbon nitride (g-C_3N_4) consists of a graphite-like layered structure and is only made of C, N, and a small quantity of H. Under ambient conditions, g-C_3N_4 is considered to be the most stable allotrope of carbon nitride and is well-known for its desirable electronic structure, which positively influences materials to work in various environmental and energy fields, and towards hydrothermal and thermal stability [30–34]. Wu et al. [31] have stated that the presence of g-C_3N_4 helps to improve the wear resistance of a system. Duan et al. [30], Wu et al. [32], and Zhu et al. [33] have stated that at elevated temperatures and extreme working conditions, the presence of g-C_3N_4 helps in the formation of a smooth, compact, and continuous transfer layer, which helps with friction coefficient stabilization and leads to a drastic decrease in wear rate. However, in a previous investigation [under review], the bulk g-C_3N_4 was observed to behave in the same way as an *abrasive*, when added in a commercial friction material composition.

Keeping this in mind, the present study focuses on the comparison of friction-wear characteristics of a low-metallic friction material when commercial graphite and an exfoliated g-C_3N_4 prepared using a tuned thermal exfoliation process are added separately in the simplified Cu-free phenolic resin-based friction mixture in the form of lubricants. The exfoliated g-C_3N_4 was produced through a special, dedicated procedure to obtain a final product which would exclusively behave as a lubricant. The prepared friction materials in the form of pins were paired with a pearlitic grey cast-iron counterface, a staple for wear tests concerning automotive friction materials. The wear tests were conducted on pin-on-disc testing equipment to obtain the friction coefficient and pin wear traces and magnitude. The worn surfaces of pins and discs and the pin cross sections were characterized using SEM/EDS. The surface roughness was obtained by the evaluation of the 3D surface topography images from laser scanning confocal microscopy. With these analyses,

a thorough evaluation of the feasibility of utilizing exfoliated g-C_3N_4 as a lubricant was conducted, when compared to graphite as a reference lubricant.

2. Materials and Methods

2.1. Materials

In this study, two types of low-metallic friction materials were produced in the form of pins. The constituents of these pins remained the same except for the type of lubricant used. Figure 1 shows the morphology of the constituents of both pins. The first type was prepared with commercial graphite as lubricant, and the second pin with exfoliated graphitic carbon nitride (codenamed as 'TEX6') as lubricant. Table 1 shows the constituents of the two friction materials with the corresponding composition of the constituents.

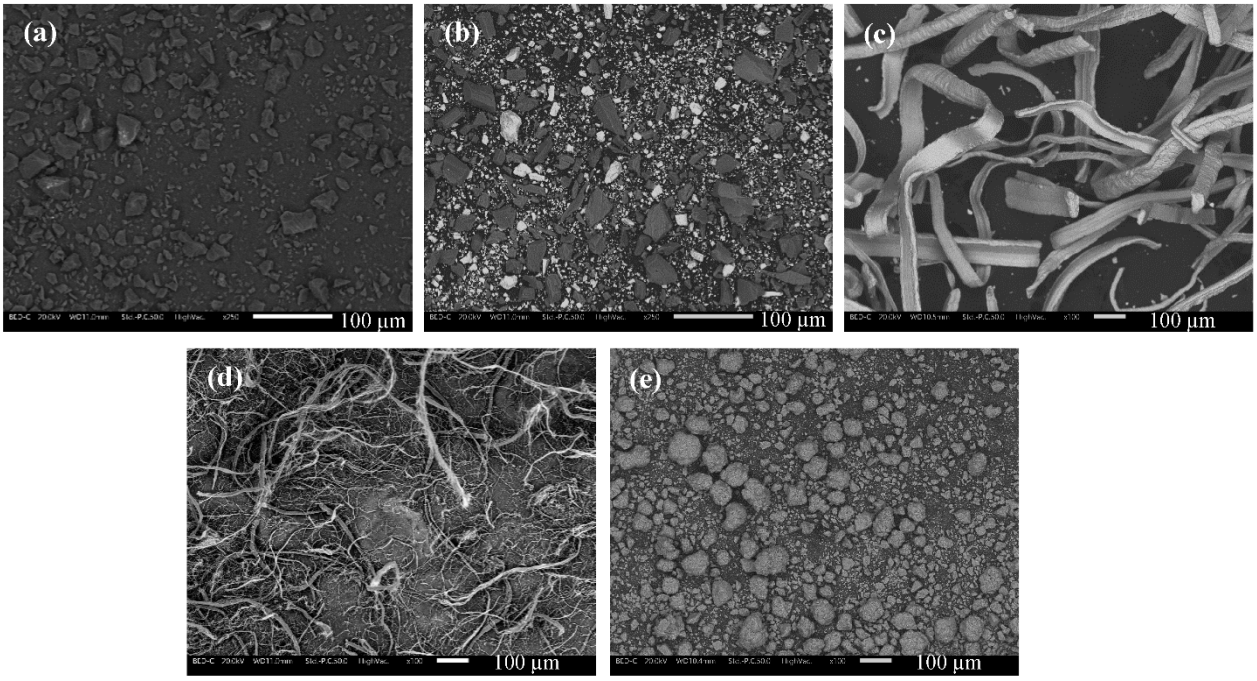

Figure 1. Morphologies of the powders used in the low-metallic pins. (**a**) Phenolic resin; (**b**) Barite and calcite; (**c**) Steel wool; (**d**) Aramid fibers; (**e**) Alumina.

Table 1. Constituents and corresponding composition of the two pins (in wt.%). BC stands for 'basic composition'.

Specimen Code Name	Phenolic Binder	Barite and Calcite	Steel Wool	Aramid Fibers	Alumina	Graphite	TEX6
BC+Graphite	8	20	22	5	30	15	–
BC+TEX6	8	20	22	5	30	–	15

The TEX6 material was prepared by the thermal exfoliation of bulk g-C_3N_4 tuned with the aim of shortening the exfoliation process. In the first step, the bulk g-C_3N_4 was prepared by the thermal polymerization of melamine in a muffle furnace. The melamine powder (from Sigma-Aldrich, St. Louis, MO, USA) was placed in a semi-closed ceramic crucible and heated for 4 h in a muffle furnace at 550 °C. The originated compact yellow product (bulk g-C_3N_4) was manually crushed using agate pestle and mortar. The specific surface area of bulk g-C_3N_4 was 8 m^2/g. In the second step, the finely crushed bulk g-C_3N_4 was spread in a thin layer on the bottom of the laboratory ceramic dish, then heated for 1 h at 600 °C in a preheated muffle furnace and immediately taken out of the furnace and cooled down at laboratory temperature. The resulting very fine powder of exfoliated g-C_3N_4 with a specific surface area of 160 m^2/g was labeled as TEX6 and used in the formulation of the friction composites.

The pins were produced through a standardized procedure. All the powders from Table 1, apart from the steel wool, were carefully weighed and mixed in a TURBULA® mixer (Muttenz, Switzerland) for 20 min. After this initial mixing, the steel wool was then added and the whole mixture was again mixed for an additional 10 min. The steel wool was added in the second step of mixing, as steel wool observes knotting and agglomeration if it is mixed for a longer period. Pins were produced from these homogeneously mixed powders through a hot-pressing procedure. The required quantity of powders was tap-pressed into a cylindrical mold of a hot-pressing apparatus (BUEHLER® hot mounting press, Lake Bluff, IL, USA), at a temperature of 150 °C, pressure of 100 MPa, and for 10 min. This procedure was followed by the post-curing process of specimens in a muffle furnace at 200 °C for 4 h. After the completion of these processes, pins with an average diameter of 10 mm and a height of 8 mm were produced. The specimens with graphite and TEX6 had an average density of 2.75 and 2.50 g/cm^3, respectively.

2.2. Testing Conditions and Methods

The pins were subjected to dry sliding tests on pin-on-disc (PoD) testing equipment (Ducom Instruments, Bengaluru, India) paired with pearlitic grey cast-iron counterface discs (diameter: 60 mm; thickness: 6 mm). Before the beginning of all tests, the discs were subjected to polishing using SiC 180-grit abrasive paper, followed by cleaning with acetone to remove any dirt, grit, and impurities. A new disc was always used for each trial. The tests were conducted at a constant loading condition of 1 MPa (79 N), sliding velocity of 1.51 m/s (600 rpm, for a track diameter of 48 mm), and at ambient/room temperature conditions (25–27 °C, temperature of the laboratory). The testing parameters were selected to replicate mild braking conditions [2,12,35]. The relative humidity of the laboratory was not controlled but regularly monitored and recorded, which typically ranged between 40–45%. To ensure the relative stability of the working conditions, all the trials were conducted within 5 days. Three individual tests with a new set of pin and disc were performed for both graphite and TEX6 containing friction composites to obtain repeatability in the results.

To achieve full conformity of the contact surfaces of pins and discs, a bedding stage was conducted at the testing parameters for 30 min. The subsequent tests were conducted for a continuous 180 min duration to establish the conditions for the proper formation of the friction layer.

The instant values of friction coefficient during the PoD tests were directly obtained from the software linked to the PoD equipment. The pin wear was obtained by weighing the pins before and after each test using an analytical balance with a precision of 10^{-4} g. The specific wear coefficient of the pin (K_a) was calculated using the equation:

$$K_a = \frac{V}{(F \times d)}$$

where V is wear volume loss; F is load applied; d is sliding distance (~8145 m).

2.3. Characterization of the Materials and Worn Surfaces

The properties and characteristics of graphite and TEX6 particles, worn top surfaces of the pins and discs, and the cross sections of the pins were characterized using a scanning electron microscope (SEM; JEOL IT300, Tokyo, Japan), equipped with Energy Dispersive X-ray Spectroscopy (EDXS; Bruker, Billerica, MA, USA) system. In the case of the pins, the maps of selected elements were obtained to understand and analyze the distribution of alloying elements. A total of six measurements were taken to obtain consistency in the analysis of the friction layer present on the pins and disc surfaces. The surface roughness of the pins after the friction tests was characterized using laser scanning confocal microscope LEXT OLS3100 (LSCM; Olympus, Tokyo, Japan). Selected regions of the friction layers of the pin specimens were also subjected to microhardness measurements, using a Vickers indenter (Future-Tech FM-310, Kawasaki, Japan), at a load of 50 g at ten different positions.

3. Results

3.1. Materials

Figure 2 represents the high-magnification images of both graphite and TEX6 lubricants tested in this study. Figure 2a,b shows the morphology of the graphite powder, which is spherical and 'flaky' in nature. Figure 2c,d represents the morphology of the TEX6 particles. In this Figure, the particles are observed to have an irregular shape and a 'fluffy' character. Additionally, as with the graphite particles, the TEX6 observes the presence of flakes as a characteristic feature.

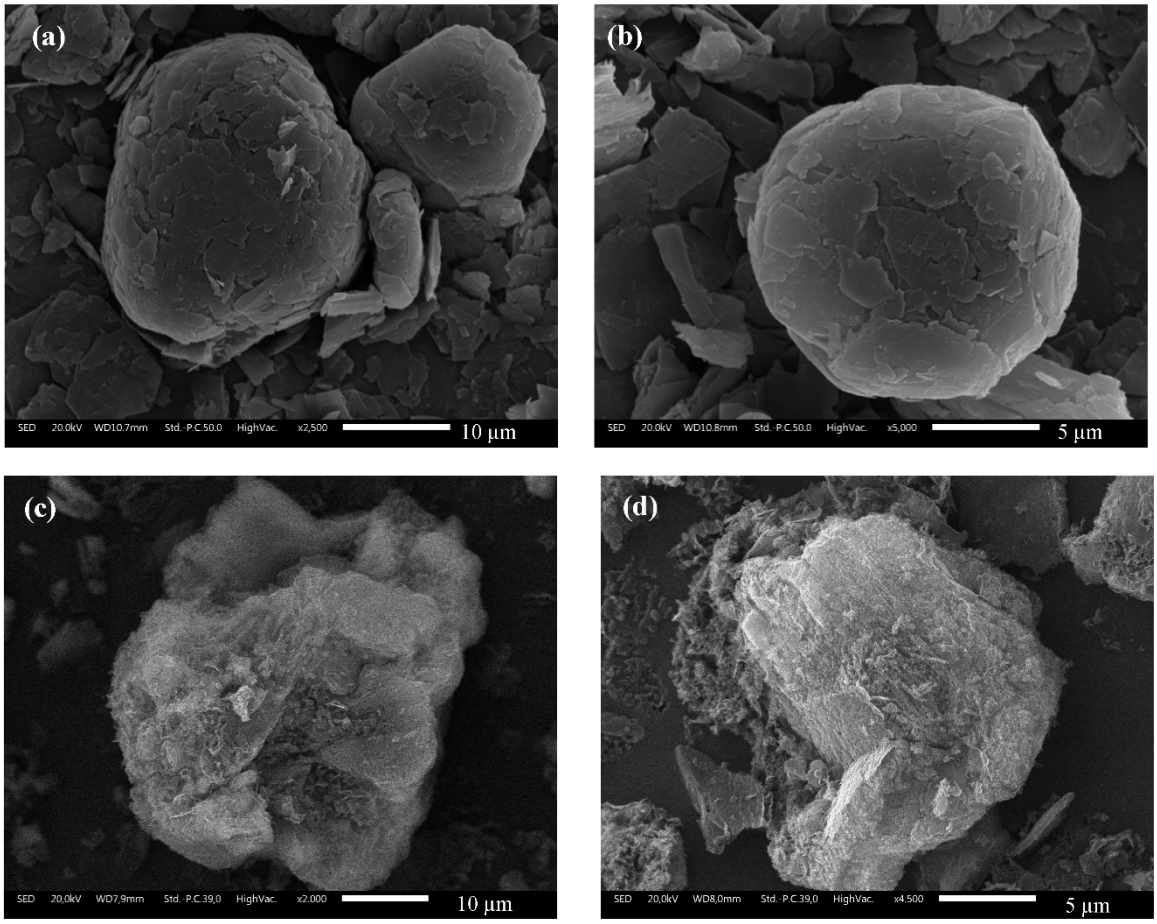

Figure 2. High-magnification particle morphology of (**a**) and (**b**) Graphite; (**c**) and (**d**) TEX6.

Figure 3 represents the cross section of the material containing TEX6. The corresponding EDXS maps of the elements are also given. The cross section observes a uniform distribution of all the constituents. It should also be noted that the distribution of TEX6 is throughout the bulk, as evidenced by the uniform distribution of C and N in respective element maps. Due to this, it is quite difficult to exactly locate the TEX6 constituent in the SEM–BED image of the material containing TEX6 in Figure 3. Similar observations were also recorded for materials containing graphite. The distribution of the constituents was highly uniform in the microstructure.

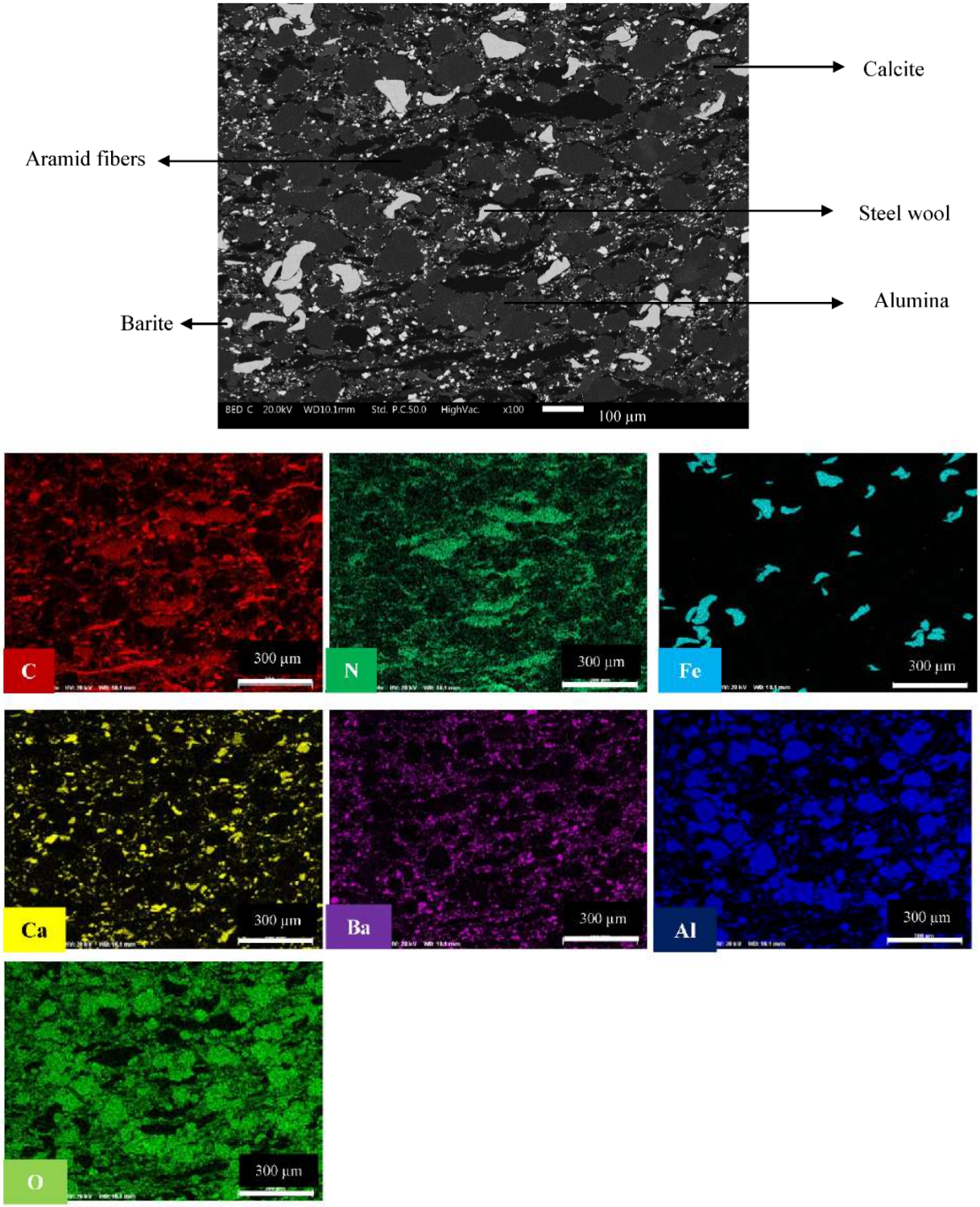

Figure 3. Cross section of the pin composition containing TEX6. The corresponding EDXS maps of the constituents are also shown.

3.2. Friction and Wear Behavior

Figure 4 depicts the typical friction traces of materials under study. In the case of the specimen containing graphite (Figure 4a), the friction trace observes considerable fluctuations, achieving a mean value close to 0.51. For material containing TEX6, Figure 4b, the friction trace observed an initial run-in up to approximately 3000 s, during which friction initially decreased and then increased to reach a steady-state value close to 0.42.

The TEX6-containing sample demonstrated a steady-state CoF trace, much better than the graphite-containing specimens, with minimal fluctuations.

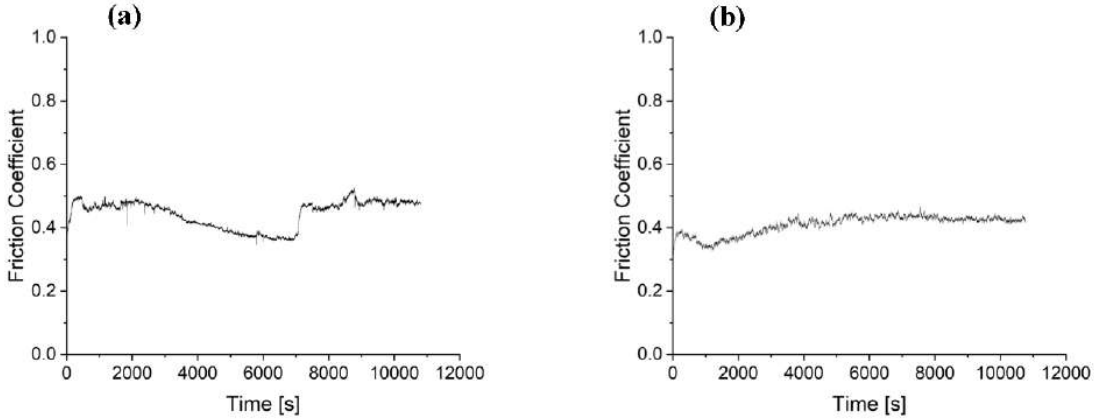

Figure 4. Friction traces of (**a**) pin containing graphite; (**b**) pin containing TEX6.

Figure 5 shows the comparison of friction coefficient (CoF, Figure 5a) and pin wear magnitude (Figure 5b) of friction composites containing graphite and TEX6. When the CoF magnitudes are compared, the graphite-containing samples have a higher average CoF magnitude, 0.51. On the other hand, the samples containing TEX6 demonstrate an appreciably lower average CoF magnitude, 0.42, when compared to graphite-containing samples. Through the plot, it can be noted that the scatter in the data is higher for the graphite-containing specimens when compared to the TEX6-filled samples.

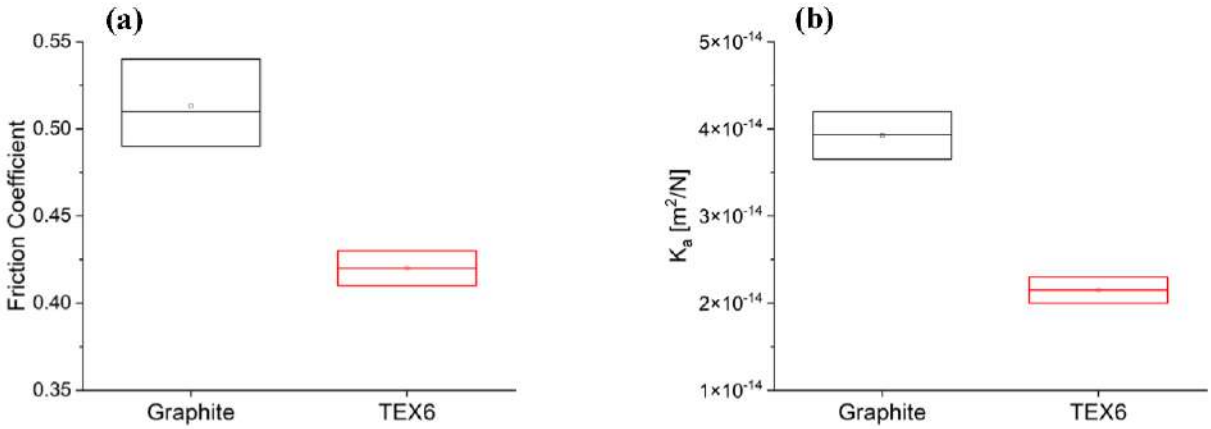

Figure 5. Comparison of (**a**) CoF magnitude; (**b**) specific wear coefficient magnitude of the pins containing graphite and TEX6.

Figure 5b shows the comparison of pin wear of both samples. Higher pin wear was observed for graphite-containing samples, reaching the specific wear coefficient of 3.93×10^{-14} m^2/N. This wear magnitude can be categorized into a 'mild-to-severe' wear regimen. Alternatively, TEX6-containing samples showed much lower wear, with a specific wear coefficient at the level of 2.15×10^{-14} m^2/N. This wear magnitude falls in the category of 'mild' wear regimen. Again, the scatter in the data of K_a for the graphite-containing specimens is higher than for the TEX6 specimens.

3.3. Analysis of Worn Pin Surfaces and Cross Sections

Figure 6 shows the worn top view images of pins containing graphite and TEX6. The corresponding EDXS maps are also reported to understand the distribution of the alloying elements on the friction surface. The white-colored/shiny regions on the worn top surface correspond to the steel fibers (as seen from the Fe maps). It is widely known that steel fibers form primary contact plateaus and aid and assist in the formation of the secondary contact plateaus. The secondary plateaus for the pins with graphite are deposited in the vicinity of the steel fibers. They are grey in color, well-compacted, and appear as smooth islands. As seen from the EDXS maps, the secondary plateaus predominantly contain Fe. An overlap in the Fe and O maps shows that the Fe in these plateaus is oxidized. When comparing both materials under this study, it is seen that in TEX6-containing samples fewer steel fibers are visible. In addition, the secondary plateaus are extremely smooth, compact, and highly extended. As in the graphite-containing materials, the secondary plateau is made of Fe oxides (evident from the overlapping of Fe and O maps). This observation was validated by the point analyses of the secondary plateaus in Table 2. An interesting aspect in this analysis is that the marker element N (which shows the presence of TEX6) was detected not only in the vicinity of the secondary plateaus (as seen in the N maps of Figure 6), but also intermixed inside the secondary plateaus (as seen in the EDXS analysis in Table 2).

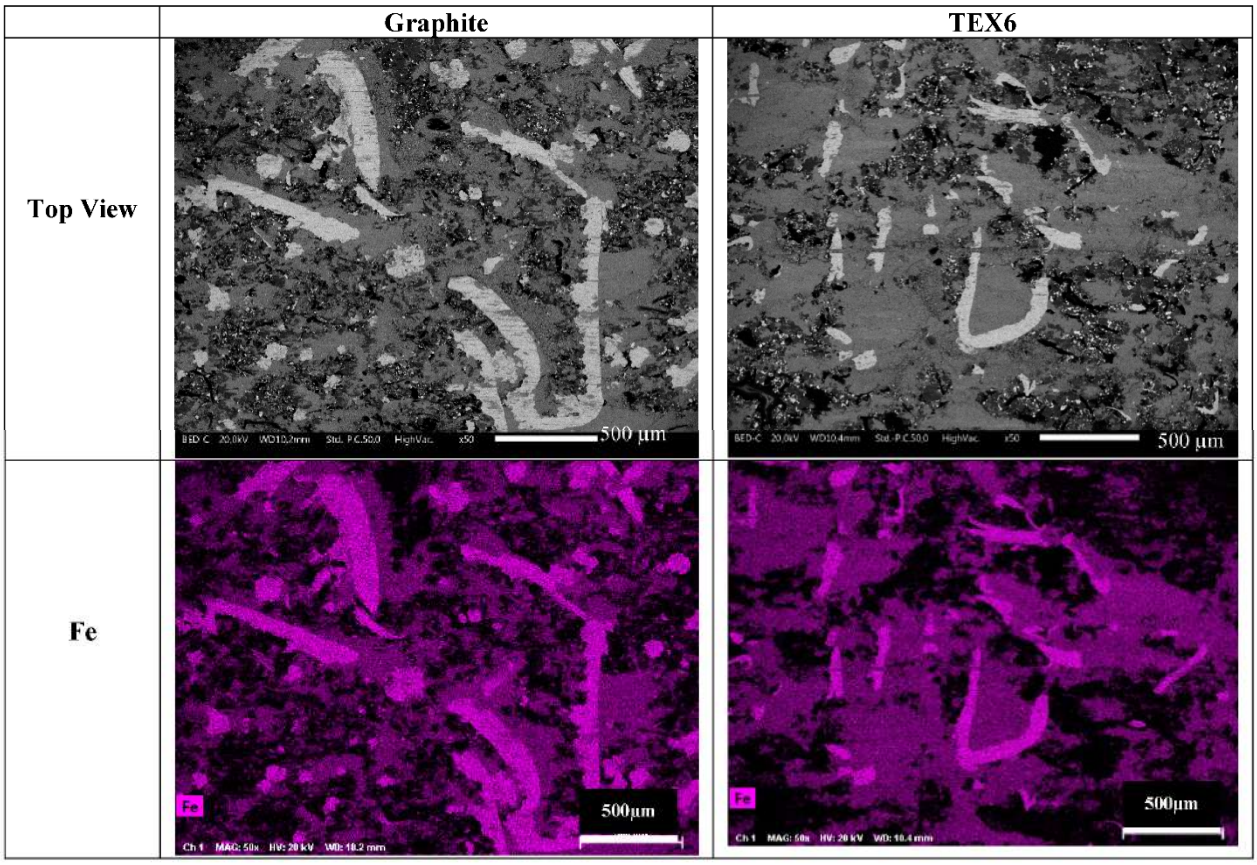

Figure 6. *Cont.*

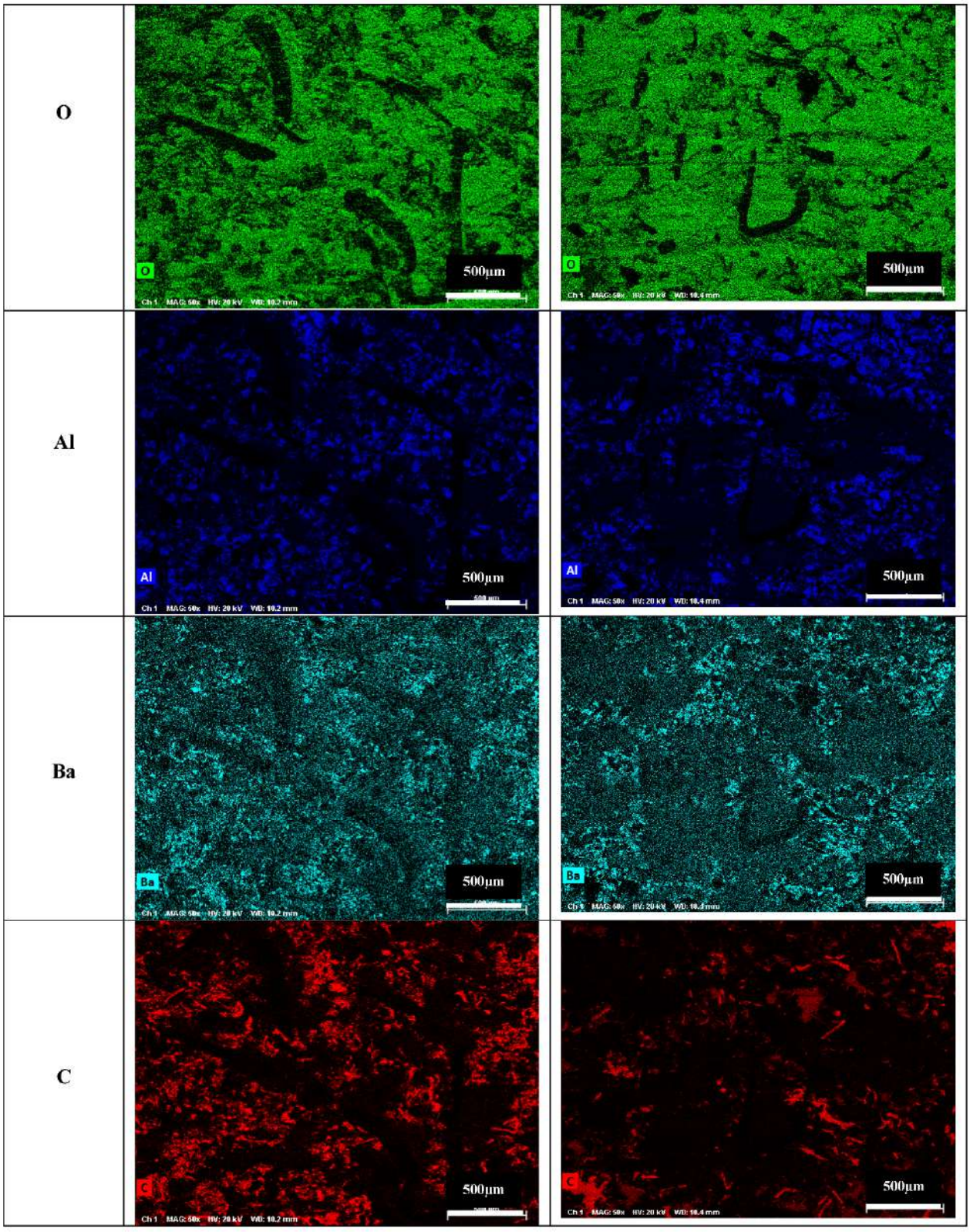

Figure 6. *Cont.*

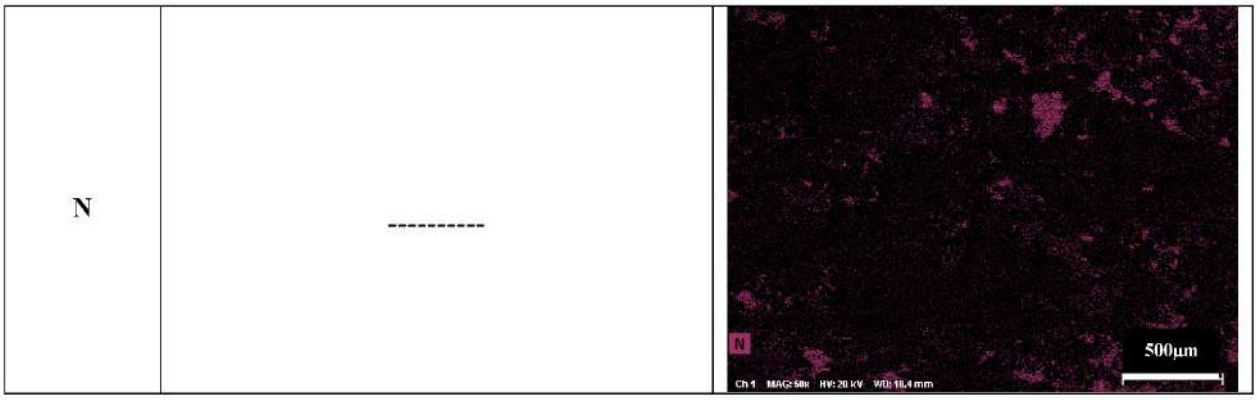

Figure 6. Worn top view and the corresponding maps of pins containing graphite and TEX6.

Table 2. Point analyses of the secondary plateau on the worn top surfaces of specimens.

Elements	Composition with Graphite	Composition with TEX6
	Point Analyses of Secondary Plateau *(Surface)*	**Point Analyses of Secondary Plateau *(Surface)***
C	8 ± 1	11 ± 0.6
N	0 ± 0	2.06 ± 0.4
Fe	51 ± 5	46 ± 4
O	33 ± 4	31 ± 1.5
Al	3.5 ± 2	6 ± 1
S	1.2 ± 0.3	0.64 ± 0.09
Ca	0.93 ± 0.18	1.1 ± 0.19
Ba	3 ± 0.9	2.36 ± 0.34

To further understand and compare the steel fiber and secondary plateau coverage in the case of both composites, a basic estimation of area was conducted on the worn top surfaces. Figure 7 shows an example of the surfaces analyzed using the ImageJ open-source software, and Table 3 provides the corresponding estimation of area. For graphite-containing specimens, as seen in both Figures 6 and 7, a dominant presence of the steel fibers is clearly observed. Regarding the secondary plateaus, it was observed that their coverage of the friction surface for TEX6-filled specimens was higher when compared to the graphite-filled samples.

Table 3. ImageJ analyses of primary and secondary plateau coverage in pins with graphite and TEX6 (from Figure 7).

Pins	Percentage Coverage Steel Fiber (%)	Percentage Coverage Secondary Plateau (%)
With Graphite	13 ± 4	23 ± 5
With TEX6	5 ± 2	40 ± 3.5

Figure 8 shows the cross section of the worn samples. As seen from the element composition obtained by point EDXS analyses (some of the analysis points shown by white circles) and presented in Table 4 as average values, the friction layers of both the specimens are predominantly composed of Fe oxides (similar to Table 2 and Figure 6). Figure 8a shows the friction layer cross sections characteristics of the graphite-filled specimen. The friction layer is marked by the arrows, and in this case, the extension of the friction layer is quite limited. Another important feature is the powdery and uncompact nature of the deposited friction layer. Alternatively, Figure 8b represents the friction layer characteristics from the cross section of the TEX6-filled specimen. From Figure 8b, it can be noticed that the friction layer is highly compact, smooth, and continuous, without the presence of powdery particles, as seen in Figure 8a for graphite-containing samples.

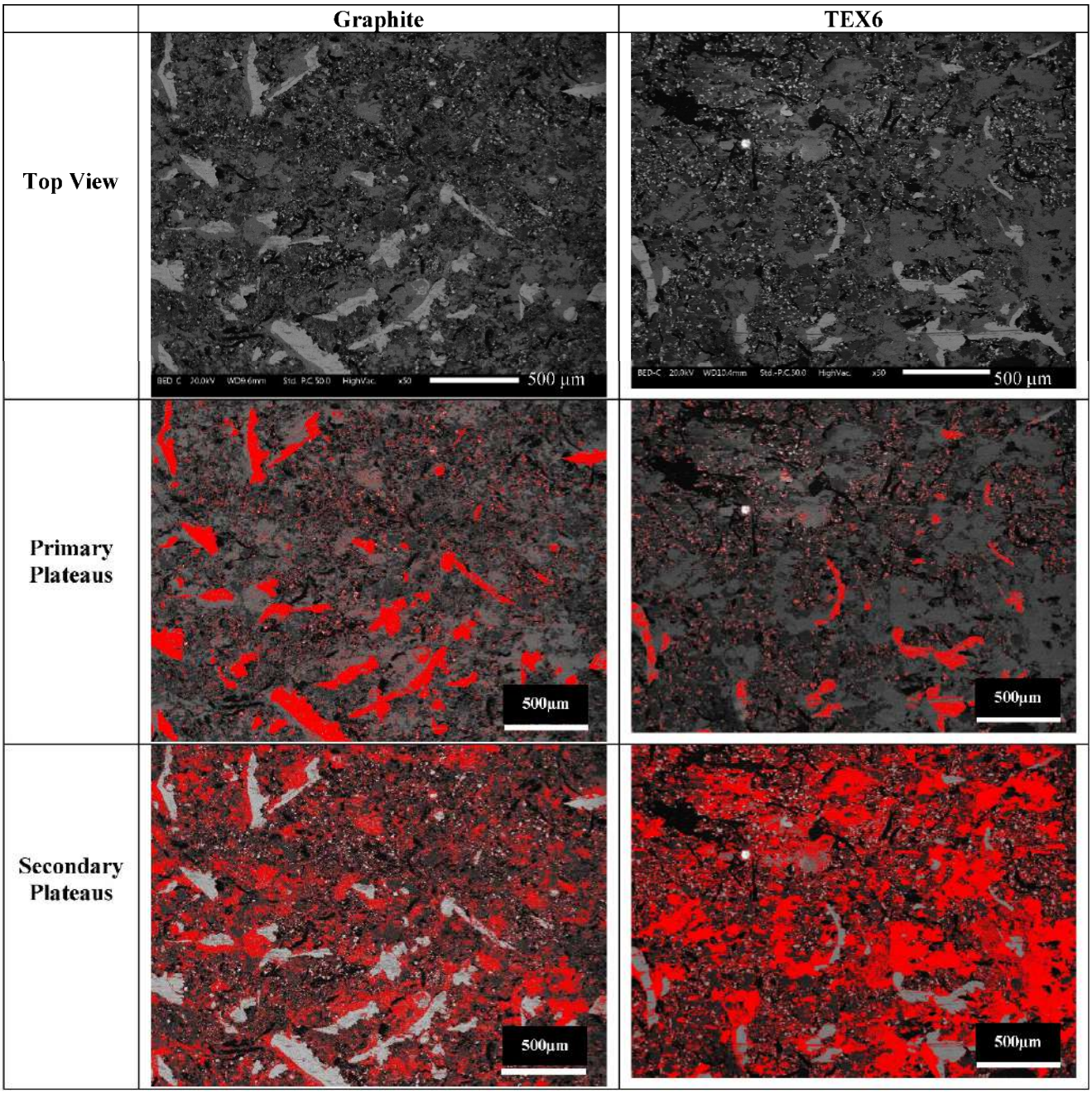

Figure 7. ImageJ analyses of the primary and secondary plateaus of pins containing graphite and TEX6.

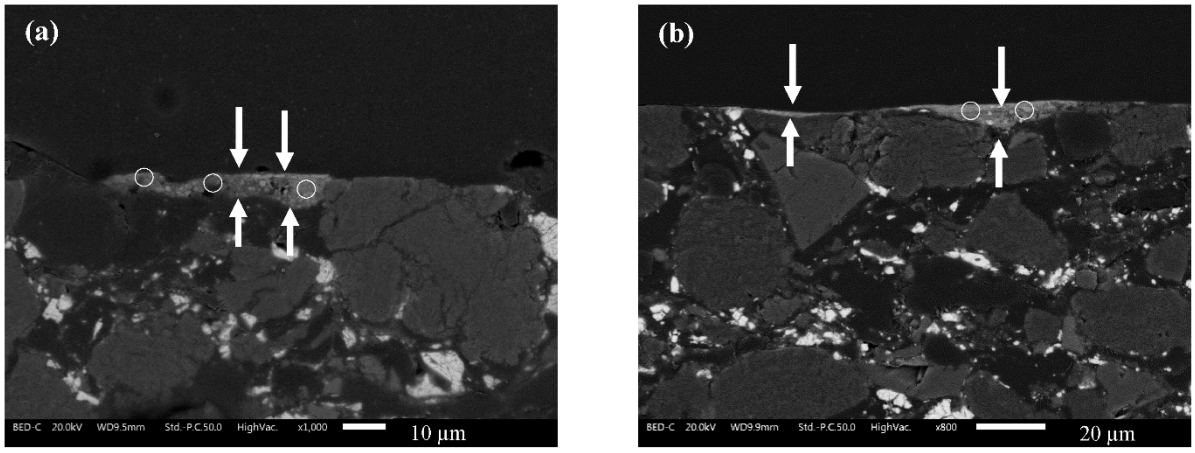

Figure 8. Cross section friction layer analyses at different locations (**a**) graphite-containing specimens; (**b**) TEX6-filled specimens. Please note the lower magnitude in (**b**) is to show the extension of the friction layer better.

Table 4. Point analyses of the friction layer from the cross section of specimens.

Elements	Composition with Graphite	Composition with TEX6
	Point Analyses of Friction Layer (Cross Section)	Point Analyses of Friction Layer (Cross Section)
C	22 ± 5	12 ± 7
N	0 ± 0	0.78 ± 0.03
Fe	41 ± 3	45 ± 5
O	25 ± 2	29 ± 2
Al	6 ± 0.6	8.5 ± 0.7
Si	0.9 ± 0.2	0.5 ± 0.7
Ca	0.6 ± 0.2	1.4 ± 0.2
Ba	4 ± 0.6	4.5 ± 0.7
Mn	0.2 ± 0.1	0 ± 0

To further understand the characteristics of the worn surfaces, the pin surfaces were subjected to microhardness analyses. The analyses were conducted on both steel fibers and the secondary plateaus. The results from the steel fibers in the samples containing graphite and TEX6 were compared with virgin steel fibers. Table 5 presents the corresponding microhardness measurements.

Table 5. Vickers microhardness measurements of virgin steel fibers, primary and secondary plateaus of graphite- and TEX6-filled specimens.

Virgin Steel Fiber (HV0.05)	Steel Fiber in Graphite Specimen (HV0.05)	Steel Fiber in TEX6 Specimen (HV0.05)	Secondary Plateaus in Graphite Specimen (HV0.05)	Secondary Plateaus in TEX6 Specimen (HV0.05)
201 ± 7	268 ± 31	256 ± 19	47 ± 6	59 ± 6

Figure 9a,b shows the surface of the steel fiber primary contact plateaus in graphite-containing specimens. The prominent presence of scratches serves as the marks of the abrasion process on the steel fiber surface. The microhardness of steel fibers as the primary contact plateaus in the case of graphite containing composites was 268 ± 31 HV0.05, showing comparatively high strain hardening due to the local large and repeated plastic deformations. Alternatively, Figure 9c,d shows the steel fiber characteristics of the TEX6-filled specimen. The absence of deep abrasion, grooving, and scratches in this composite can be observed. The microhardness values of the primary contact plateaus measured for

TEX6 containing composites were lower: 256 ± 19 HV0.05. Lastly, Figure 9e,f shows the back-scattered electron images of secondary contact plateaus, deposited around the steel fiber, for graphite-(Figure 9e) and TEX6 (Figure 9f)-filled specimens. In the case of graphite-containing specimens, the presence of small patches/islands of secondary plateaus can be seen. To a great extent, these secondary contact plateaus are not well-compacted and are powdery in nature. For TEX6 specimens, a large extension of deposited secondary contact plateaus can be seen around the steel fiber. In the case of TEX6-containing samples, the predominant presence of large areas of compacted secondary plateaus, smooth and continuous, can also be observed. The corresponding microhardness value of the secondary plateaus of TEX6 specimens is higher, reaching 59 ± 6 HV0.05, when compared to graphite-containing specimens, achieving the value 47 ± 6 HV0.05 (Table 5). This observation confirms the higher compactness of the secondary plateaus in the worn TEX6 specimens.

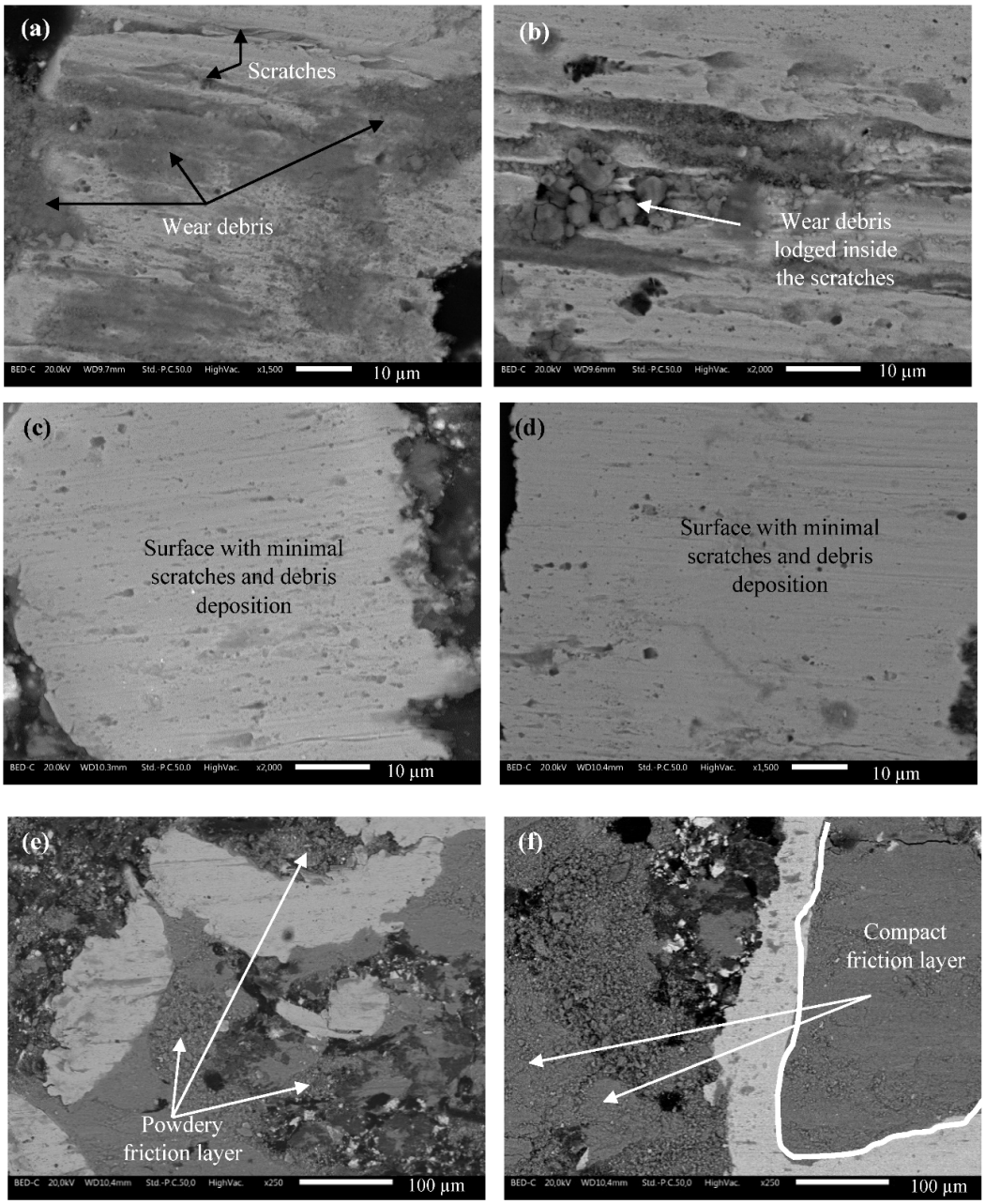

Figure 9. High-magnification images of (**a**,**b**) steel fibers on the worn surfaces of graphite-containing specimens; (**c**,**d**) steel fibers on the worn surfaces of TEX6-filled specimens; (**e**,**f**) secondary plateaus deposited on the worn surfaces of graphite and TEX6 specimens, respectively.

Lastly, the worn pin surfaces were subjected to analyses on a laser scanning confocal microscope (LSCM) to evaluate the surface roughness. Figure 10a,b shows the images of the friction surfaces of graphite- and TEX6-containing specimens, respectively, obtained in light microscopy mode. The corresponding height maps obtained in confocal mode are shown in Figure 10c,d. The surface of the TEX6-containing sample is smoother, as evident from the height maps of both samples. The arithmetical mean roughness values (R_a) were calculated as the average of the R_a obtained in ten profiles perpendicular to the sliding direction. A significantly lower R_a value was obtained for TEX6 samples when compared to the graphite specimens.

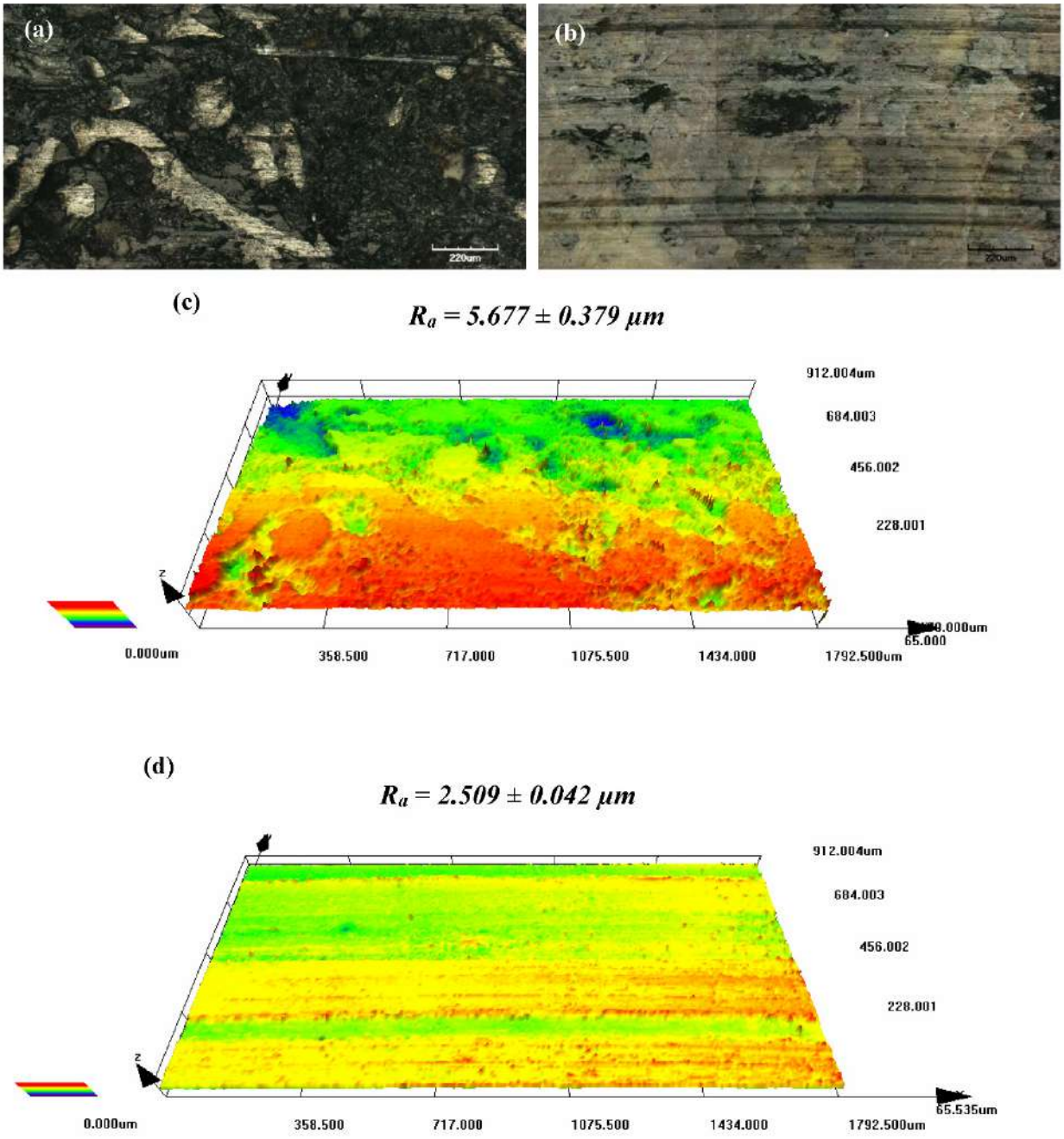

Figure 10. (**a**,**b**) Surface images of graphite and TEX6 samples, respectively subjected to LSCM analyses; (**c**) Height map of specimen containing graphite; (**d**) Height map of TEX6-filled samples.

3.4. Analysis of Worn Disc Surface

Figure 11 show the worn top view of the discs paired with graphite-(Figure 11a) and TEX6 (Figure 11b)-containing specimens. In the first case, the counterface is covered with abrasive scratches. In the second case, the surface is covered by streaks of the grey transfer layer. This transfer layer is the friction layer, made of both discs (Fe, Mn) and pin (Fe, Al, Ba, and Ca) constituents. However, as with the pin friction layer, the disc friction layer is also predominantly made of oxides of Fe, which was revealed through a point EDXS analysis.

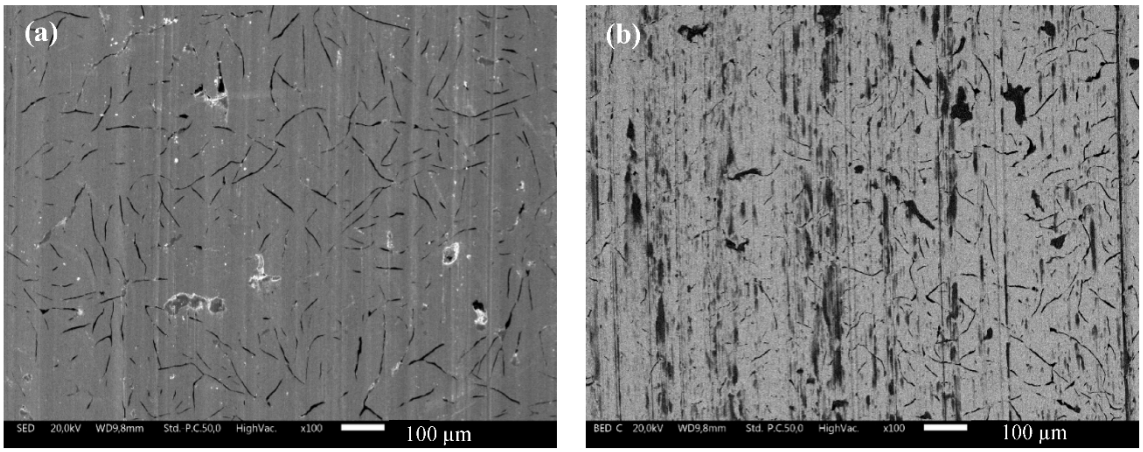

Figure 11. Worn top view of disc surface (**a**) paired with graphite-containing specimens; (**b**) TEX6-filled specimens.

4. Discussion

A summary of the experimental observations for both graphite- and TEX6-containing samples is shown in Table 6.

Table 6. Summary table of the experimental observations for both graphite- and TEX6-containing specimens.

Study/Characterization	Graphite-Containing Samples	TEX6-Containing Samples
Distribution of composition in cross section	Well-distributed and densified specimens with both lubricants	
Friction coefficient trends and magnitude	Fluctuating traces around an average CoF magnitude of 0.51	Smooth steady-state friction trace, with CoF magnitude of 0.42
Pin wear	'Mild-to-severe' wear regime	'Mild' wear regime
Primary plateaus (steel fibers)	Abrasive scratches, high strain hardening	Minimal scratches and limited strain hardening; surface steel fibers largely covered by the secondary plateau
Secondary plateaus (compacted debris)	Lower extension and compactness	Higher extension and compactness
Friction layer (cross section)	Limited extension, powdery and uncompact below the surface	Higher extension, highly compacted, and smooth
Surface roughness of worn pin surfaces	High	Low
Characteristics of the worn surfaces of paired discs	High scratches/abrasions without any transfer on the surface	Considerable transfer on the disc surface

Graphite particles are typically used as lubricant additives in commercial friction materials with optimized formulations. In the present investigation, a simplified formulation is used with a limited number of ingredients to better understand the individual role of the lubricant additions. The obtained results, summarized in Table 6, clearly show that the friction and wear performances of the TEX6-containing material are better than those displayed by the graphite-containing samples. This means that in our simplified material formulation, the exfoliated g-C_3N_4 (TEX6) particles were able to exert a better lubricating performance than the selected commercial graphite.

Both graphite and the exfoliated g-C_3N_4 (TEX6) particles are exceptionally layered materials with highly preferred layer orientation. The better lubricating performance of TEX6 relates to its finer structure, which is evident in Figure 2. The 'fluffy' particles of TEX6 easily disintegrate during the friction process to form very fine wear particles, which actively contribute to the formation of the secondary contact plateaus (as seen in Figure 6). The presence of a smooth surface of worn TEX6 samples was also demonstrated by the LSCM analysis in Figure 10b. The friction layers are subjected to large shear stress during dry sliding. The TEX6 particles in the secondary plateaus can better accommodate the local strains, favoring the relative motion and subsequent compaction of the wear debris [24]. This hypothesis is in good agreement with the work of Rajan et al. [36], who studied the effect of graphene (that has a structural similar to the exfoliated g-C_3N_4 particles) in friction composites and observed its positive effect on the stabilization of the CoF and the decrease of wear rate.

A higher hardness of secondary contact plateaus recorded for TEX6-containing composites is a result of better compaction of secondary contact plateaus, resulting in their improved stability. Consequently, the pin wear for TEX6 pins were much lower than the graphite-containing pins. Additionally, a smooth evolution of the friction coefficient in the steady state, without the large fluctuations, was observed for the TEX6 specimen, which was uncharacteristic of the friction traces in graphite-containing material. From Figure 9b, for the worn pin surface of the graphite-containing sample, the wear debris was locked in the formed scratches, originating from the disruption of the neighboring secondary plateaus [37]. The presence of this lodged wear debris enhanced the abrasive character of the friction contact, leading to considerable abrasive wear of the paired disc surface (Figure 11a). The presence of this lodged wear debris (and its subsequent dynamic disengagement) between the interfaces could potentially lead to disruption of the secondary contact plateaus (low secondary plateau coverage shown in Table 3), fluctuation in the CoF traces (Figure 4a), higher pin wear, and elevated average CoF (Figure 5). These observations are also confirmed by the LSCM analysis, which noted high surface roughness of the worn graphite-containing sample in Figure 10a. The locked wear debris were mainly Fe oxides, as was observed from the point EDXS analysis.

Through these preliminary studies, the addition of exfoliated g-C_3N_4 (TEX6) particles in a basic friction material formulation observed promising results, both in terms of friction and wear behavior and secondary plateau formation, with respect to the formulation containing commercial graphite particles. As already mentioned, the selected formulation was simplified and not optimized. This explains the poor performance obtained with the addition of the commercial graphite. However, this also highlights the good performance of the newly developed exfoliated g-C_3N_4 particles, thereby paving the path for further testing and analyses.

5. Conclusions

A simplified Cu-free phenolic resin-based friction material composition was subjected to dry sliding tests on pin-on-disc testing equipment by varying the type of lubricant used in the material composition. The lubricants tested were graphite and exfoliated g-C_3N_4 particles (TEX6) prepared by tuned thermal exfoliation of bulk g-C_3N_4.

- The TEX6-containing specimens showed the presence of a smooth, compact, and extended secondary plateau on the worn surfaces. This was verified by the high microhardness of the secondary plateaus. This property was attributed to the TEX6 particle structure. Due to its inherent 'fluffy' nature, the TEX6 particles could disintegrate easily into fine wear particles, contributing to the formation of a robust secondary plateau. The presence of a stable and high-quality secondary contact plateau led to the reduction in the pin wear of TEX6 specimens. Observed lubricating properties of the exfoliated g-C_3N_4 (TEX6) differs in comparison to bulk g-C_3N_4, which shows a mildly abrasive character when added to commercial friction material, as observed by Matějka et al. [38].

- The steel fibers on the worn graphite-containing specimens observed scratches, which had wear debris lodged in them. A consequent interaction with this wear debris caused abrasion/scratches on the disc surface [6,37]. A subsequent potential detachment of this debris and its interaction with the mating surfaces led to instability in CoF, high pin wear, and a discontinuous and powdery secondary contact plateau [3,4]. Alternatively, the TEX6-containing sample did not observe any scratches on the steel fiber surfaces, promoting low pin wear, stable and low CoF, and higher extension of the friction layer both on the pin and disc surfaces—typical characteristics of lubricants [5,17,20,25,30,35].
- The initial testing of TEX6 in a basic friction material composition demonstrated its potential functionality as a lubricant, pending further study and analysis through specific dynamometric bench tests to obtain additional data regarding its suitability in the formulation of Cu-free brake pads.

Author Contributions: Investigation, P.J., K.F.; Writing—Original Draft, P.J.; Discussion, P.J., V.M., G.S.; Writing—Review and Editing, V.M., G.S.; Conceptualization, G.S., P.J., V.M.; Data treatment, P.J., K.F.; Methodology, P.J., V.M., G.S.; Software, P.J., V.M.; Validation, V.M., G.S.; Supervision, G.S. All authors have read and agreed to the published version of the manuscript.

Funding: This work was supported by VŠB-TU Ostrava (Project No. SP 2022/61).

Institutional Review Board Statement: Not applicable.

Informed Consent Statement: Not applicable.

Data Availability Statement: Data presented in this study are available on request from the corresponding author.

Conflicts of Interest: The authors declare no conflict of interest.

References

1. Yun, R.; Filip, P.; Lu, Y. Performance and evaluation of eco-friendly brake friction materials. *Tribol. Int.* **2010**, *43*, 2010–2019. [CrossRef]
2. Leonardi, M.; Menapace, C.; Matějka, V.; Gialanella, S.; Straffelini, G. Pin-on-disc investigation on copper-free friction materials dry sliding against cast iron. *Tribol. Int.* **2018**, *119*, 73–81. [CrossRef]
3. Kukutschová, J.; Roubíček, V.; Mašláň, M.; Jančík, D.; Slovák, V.; Malachová, K.; Pavlíčková, Z.; Filip, P. Wear performance and wear debris of semimetallic automotive brake materials. *Wear* **2010**, *268*, 86–93. [CrossRef]
4. Straffelini, G.; Maines, L. The relationship between wear of semimetallic friction materials and pearlitic cast iron in dry sliding. *Wear* **2013**, *307*, 75–80. [CrossRef]
5. Antonyraj, I.J.; Singaravelu, D.L. Tribological characterization of various solid lubricants based copper-free brake friction materials-A comprehensive study. *Mater. Today Proc.* **2019**, *27*, 2650–2656. [CrossRef]
6. Prabhu, T.R. Effects of solid lubricants, load, and sliding speed on the tribological behavior of silica reinforced composites using design of experiments. *J. Mater.* **2015**, *77*, 149–160. [CrossRef]
7. Talib, R.J.; Muchtar, A.; Azhari, C.H. Microstructural characteristics on the surface and subsurface of semimetallic automotive friction materials during braking process. *J. Mater. Process. Technol.* **2003**, *140*, 694–699. [CrossRef]
8. Cho, M.H.; Cho, K.H.; Kim, S.J.; Kim, D.H.; Jang, H. The role of transfer layers on friction characteristics in the sliding interface between friction materials against gray iron brake disks. *Tribol. Lett.* **2005**, *20*, 101–108. [CrossRef]
9. Tavangar, R.; Moghadam, H.A.; Khavandi, A.; Banaeifar, S. Comparison of dry sliding behavior and wear mechanism of low metallic and copper-free brake pads. *Tribol. Int.* **2020**, *151*, 106416. [CrossRef]
10. Straffelini, G. *Friction and Wear: Methodologies for Design and Control*; Springer: Berlin/Heidelberg, Germany, 2015; ISBN 978-3-319-05894-8.
11. Neis, P.D.; Ferreira, N.F.; Fekete, G.; Matozo, L.T.; Masotti, D. Towards a better understanding of the structures existing on the surface of brake pads. *Tribol. Int.* **2017**, *105*, 135–147. [CrossRef]
12. Menapace, C.; Leonardi, M.; Matějka, V.; Gialanella, S.; Straffelini, G. Dry sliding behavior and friction layer formation in copper-free barite containing friction materials. *Wear* **2018**, *398–399*, 191–200. [CrossRef]
13. Boz, M.; Kurt, A. The effect of Al_2O_3 on the friction performance of automotive brake friction materials. *Tribol. Int.* **2007**, *40*, 1161–1169. [CrossRef]
14. Tang, C.F.; Lu, Y. Combinatorial Screening of Ingredients for Steel Wool Based Semimetallic and Aramid Pulp Based Nonasbestos Organic Brake Materials. *J. Reinf. Plast. Compos.* **2004**, *23*, 51–63. [CrossRef]

15. Qu, X.; Zhang, L.; Ding, H.; Liu, G. The Effect of Steel Fiber Orientation on Frictional Properties of Asbestos-Free Friction Materials. *Polym. Compos.* **2004**, *25*, 94–101. [CrossRef]
16. Aranganathan, N.; Mahale, V.; Bijwe, J. Effects of aramid fiber concentration on the friction and wear characteristics of non-asbestos organic friction composites using standardized braking tests. *Wear* **2016**, *354–355*, 69–77. [CrossRef]
17. Cho, M.H.; Ju, J.; Kim, S.J.; Jang, H. Tribological properties of solid lubricants (graphite, Sb2S3, MoS2) for automotive brake friction materials. *Wear* **2006**, *260*, 855–860. [CrossRef]
18. Tomášek, V.; Kratošová, G.; Yun, R.; Fan, Y.; Lu, Y. Effects of alumina in nonmetallic brake friction materials on friction performance. *J. Mater. Sci.* **2009**, *44*, 266–273. [CrossRef]
19. Baskara Sethupathi, P.; Chandradass, J. Comparative study of different solid lubricants towards friction stability in a non-asbestos disc brake pad. *Ind. Lubr. Tribol.* **2021**, *73*, 897–903.
20. Justin Antonyraj, I.; Vijay, R.; Lenin Singaravelu, D. Influence of WS2/SnS2 on the tribological performance of copper-free brake pads. *Ind. Lubr. Tribol.* **2019**, *71*, 398–405.
21. Sathickbasha, K.; Selvakumar, A.S.; Balachandran, S.R.; Hariharasakthisudhan, P. Multi-metal sulfide pre-blend combination on the tribological performance of the brake friction material. *Ind. Lubr. Tribol.* **2021**, *73*, 235–334.
22. Sathickbasha, K.; Selvakumar, A.S.; Balaji, M.A.S.; Rajan, B.S. The dual role of metal sulfides as lubricant and abrasive: An interface study in friction composite. *Mater. Res. Express* **2019**, *6*, 045315. [CrossRef]
23. Sugözü, İ.; Sugözü, B. Investigation of The Effect of Solid Lubricant Particle Sizes on Friction and Wear Properties in Friction Composites: An Experimental Case Study with Graphite. *Int. J. Automot. Sci. Technol.* **2021**, *5*, 179–183. [CrossRef]
24. Österle, W.; Dmitriev, A.I. The role of solid lubricants for brake friction materials. *Lubricants* **2016**, *4*, 5. [CrossRef]
25. Ertan, R.; Yavuz, N. The effects of graphite, coke and ZnS on the tribological and surface characteristics of automotive brake friction materials. *Ind. Lubr. Tribol.* **2011**, *63*, 245–253. [CrossRef]
26. Kim, S.J.; Hyung Cho, M.; Hyung Cho, K.; Jang, H. Complementary effects of solid lubricants in the automotive brake lining. *Tribol. Int.* **2007**, *40*, 15–20. [CrossRef]
27. Asmoro, G.; Surojo, E.; Ariawan, D.; Muhayat, N.; Raharjo, W.W. Role of solid lubricant (MoS2 and graphite) variations on characteristics of brake lining composite. *IOP Conf. Ser. Mater. Sci. Eng.* **2018**, *420*, 012022. [CrossRef]
28. Zhang, E.; Gao, F.; Fu, R.; Lu, Y.; Han, X.; Su, L. Tribological behavior of phenolic resin-based friction composites filled with graphite. *Materials* **2021**, *14*, 742. [CrossRef] [PubMed]
29. Cheng, Z.L.; Qin, X.X. Study on friction performance of graphene-based semi-solid grease. *Chin. Chem. Lett.* **2014**, *25*, 1305–1307. [CrossRef]
30. Duan, C.; Yuan, D.; Yang, Z.; Li, S.; Tao, L.; Wang, Q.; Wang, T. High wear-resistant performance of thermosetting polyimide reinforced by graphitic carbon nitride (g-C3N4) under high temperature. *Compos. Part A Appl. Sci. Manuf.* **2018**, *113*, 200–208. [CrossRef]
31. Wu, L.; Zhang, Z.; Yang, M.; Yuan, J.; Li, P.; Guo, F.; Men, X. One-step synthesis of g-C3N4 nanosheets to improve tribological properties of phenolic coating. *Tribol. Int.* **2019**, *132*, 221–227. [CrossRef]
32. Wu, L.; Zhang, Z.; Yang, M.; Yuan, J.; Li, P.; Guo, F.; Men, X. Facile synthesis of CuO/g-C3N4 hybrids for enhancing the wear resistance of polyimide composite. *Eur. Polym. J.* **2019**, *116*, 463–470. [CrossRef]
33. Zhu, L.; Wang, Y.; Hu, F.; Song, H. Structural and friction characteristics of g-C 3 N 4 /PVDF composites. *Appl. Surf. Sci.* **2015**, *345*, 349–354. [CrossRef]
34. Gaddam, S.K.; Pothu, R.; Boddula, R. Graphitic carbon nitride (g-C3N4) reinforced polymer nanocomposite systems—A review. *Polym. Compos.* **2020**, *41*, 430–442. [CrossRef]
35. Leonardi, M.; Alemani, M.; Straffelini, G.; Gialanella, S. A pin-on-disc study on the dry sliding behavior of a Cu-free friction material containing different types of natural graphite. *Wear* **2020**, *442–443*, 203157. [CrossRef]
36. Surya Rajan, B.; Sai Balaji, M.A.; Mohamed Aslam Noorani, A.B. Tribological performance of graphene/graphite filled phenolic composites—A comparative study. *Compos. Commun.* **2019**, *15*, 34–39.
37. Matějka, V.; Lu, Y.; Fan, Y.; Kratošová, G.; Lešková, J. Effects of silicon carbide in semi-metallic brake materials on friction performance and friction layer formation. *Wear* **2008**, *265*, 1121–1128. [CrossRef]
38. Matějka, V.; Leonardi, M.; Praus, P.; Straffelini, G.; Gialanella, S. The Role of Graphitic Carbon Nitride in the Formulation of Copper-Free Friction Composites Designed for Automotive Brake Pads. *Metals* **2022**, *12*, 123. [CrossRef]